Journal of Sound and Vibration 331 (2012) 4057–4071

Contents lists available at SciVerse ScienceDirect

Journal of Sound and Vibration

journal homepage: www.elsevier.com/locate/jsvi

On the comparison of semi-analytical methods for the stability analysis of delay differential equations

Dennis J. Tweten*, Genevieve M. Lipp, Firas A. Khasawneh, Brian P. Mann

Mechanical Engineering and Materials Science Department, Duke University, Durham, NC 27708, United States

ARTICLE INFO

Article history:
Received 4 August 2011
Received in revised form
6 March 2012
Accepted 11 April 2012
Handling Editor: K. Worden
Available online 3 May 2012

ABSTRACT

This paper provides the first comparison of the semi-discretization, spectral element, and Legendre collocation methods. Each method is a technique for solving delay differential equations (DDEs) as well as determining regions of stability in the DDE parameter space. We present the necessary concepts, assumptions, and equations required to implement each method. To compare the relative performance between the methods, the convergence rate and computational time for each method is compared in three numerical studies consisting of a ship stability example, the delayed damped Mathieu equation, and a helicopter rotor control problem. For each study, we present one or more stability diagrams in the parameter space and one or more convergence plots. The spectral element method is demonstrated to have the quickest convergence rate while the Legendre collocation method requires the least computational time. The semi-discretization method on the other hand has both the slowest convergence rate and requires the most computational time.

1. Introduction

It has been known for quite some time that several systems can be described by models that include past effects. These systems, where the rate of change in a state is determined by both the past and the present states, are described by delay differential equations (DDEs). While theoretical investigations of DDEs are typically more involved than those of ordinary differential equations, due to the growth in the state space from a finite dimension to an infinite dimension [1,2], it is interesting to point out that delays often present a more feasible modeling alternative than attempting to include the physics of very complex phenomena or processes that may have unknown physics, e.g. sound reverberation physics, gene expression dynamics, or diffusion [3–6]. Further examples from recent literature include active vibration absorbers for dynamic structures [7–9], machine tool chatter in manufacturing processes [10–13], and the stability of periodically forced columns [14].

Many analysis methods have appeared in the literature for studying delay equations. For example, the stability of DDEs has been studied using D-subdivision [15], continuous time approximation (CTA) [16–18], and the cluster treatment of characteristic roots methods (CTCR) [19,20]. The focus in D-subdivision and the CTCR methods is on charting the stability boundaries by investigating the characteristic polynomial of DDEs. Whereas CTCR can find the stability of a wide class of autonomous delay equations, the D-subdivision method is confined to a much smaller class of DDEs, namely systems of

* Corresponding author. Tel.: +1 919 660 5338; fax: +1 919 660 8963.
E-mail addresses: dennis.tweten@duke.edu (D.J. Tweten), genevieve.lipp@duke.edu (G.M. Lipp), firas.khasawneh@duke.edu (F.A. Khasawneh), brian.mann@duke.edu (B.P. Mann).

0022-460X/$ - see front matter © 2012 Elsevier Ltd. All rights reserved.
http://dx.doi.org/10.1016/j.jsv.2012.04.009

any order with either very little or no damping [15]. On the other hand, the CTA method converts the DDE into an equivalent high- and finite-dimensional state space, and it can yield both the stability and equilibria of the underlying DDE. Nevertheless, for some DDEs the CTA method can produce very large matrices leading to significant computational difficulties. A common limitation of all the above methods is that they have only been applicable to autonomous DDEs.

Several recent works have proposed discretization methods to ascertain the stability properties of both autonomous and non-autonomous DDEs. For example, several works have described a semi-discretization approach, which divides the time-line into short intervals on which an approximate analytical solution can be obtained [21–23]. The collection of the approximate analytical solutions is then used to create a finite-dimensional transition matrix, which approximates the infinite-dimensional monodromy operator of the DDE. Collocation methods have also appeared in the literature using either Chebyshev or LGL points to construct a dynamic map that approximates the DDE [24]. As yet another example, the Temporal Finite Element Analysis (TFEA) method has been used to study the stability of equilibria of DDEs [25]. This method discretizes the time interval of interest into a finite number of temporal elements. The original DDE is then transformed into the form of a discrete map whose characteristic multipliers determine stability. While the original versions of this approach focused solely on *h*-convergence, by simply increasing the number of temporal elements, more recent versions, referred to as spectral element methods, have demonstrated both *p*- and *hp*-convergence methodologies [26].

Although the semi-discretization, collocation, and spectral element methods have all been used to study various DDEs, a comparison amongst these methods has yet to appear in the literature. In contrast to recent works on the spectral element method [26–29] which sought to develop this technique, the focus of the present manuscript is to compare and contrast the features of the three techniques along with their performance. In particular, the convergence rate and the computational time required to generate a converged stability diagram are compared using three numerical studies.

The content of this paper is organized as follows. The next section describes the assumptions and equations required to implement each method, followed by the section which discusses the criteria used to compare the methods and how the criteria was implemented. Three numerical studies are then presented which include a ship stability model, the delayed damped Mathieu equation, and a helicopter rotor control problem. Finally, the conclusions of the numerical study are presented.

2. Description of methods

A general delay differential equation can be written in the state-space form according to

$$\dot{\mathbf{x}}(t) = \mathbf{A}(t)\mathbf{x}(t) + \mathbf{B}(t)\mathbf{x}(t-\tau), \tag{1}$$

where $\mathbf{x}$ is a d-dimensional vector, $\mathbf{A}(t)$ and $\mathbf{B}(t)$ are the $d \times d$ system matrices, and τ is a positive delay. Eq. (1) can describe the dynamics of a linear delay oscillator, or it can represent the linearization of a non-linear system about an equilibrium position. Two specific cases of DDEs are of special interest: the autonomous DDE case (i.e. $\mathbf{A}(t) = \mathbf{A}$, $\mathbf{B}(t) = \mathbf{B}$) and the non-autonomous case where the coefficients are time periodic with the period T (i.e. $\mathbf{A}(t) = \mathbf{A}(t+T)$, $\mathbf{B}(t) = \mathbf{B}(t+T)$). The case $\tau = T$ is of special interest in science and engineering and it appears in a wide variety of applications such as machining. This paper focuses on describing stability analysis techniques for DDEs such as Eq. (1) for both autonomous and time-periodic DDEs with $\tau = T$.

The stability analysis of the equilibria of DDEs can be performed using Floquet theory. This approach investigates the spectrum of the monodromy operator which maps the history segment of $[-\tau,0]$ one period ahead onto $[-\tau+T,T]$ which becomes $[0,T]$ for the case where $\tau = T$, see Fig. 1a. However, the monodromy operator acts on an infinite dimensional state space: the space of continuous functions. Therefore, in general, it is not possible to deal directly with the eigenvalues of the monodromy operator. Instead we approximate the eigenvalues of the monodromy operator with the eigenvalues of a finite dimensional matrix called the monodromy matrix. The monodromy matrix $\mathbf{U}$ represents the linear map

$$\mathbf{x}_{k+1} = \mathbf{U}\mathbf{x}_k, \tag{2}$$

between the discretized state-space over the segment $[-T,0]$ denoted by the vector $\mathbf{x}_k$ and those over the segment $[0,T]$, represented by the vector $\mathbf{x}_{k+1}$, see Fig. 1b. As the discretization is refined, the size of $\mathbf{U}$ is increased while more eigenvalues are well approximated. The eigenvalues of the monodromy matrix form an approximation to the Floquet multipliers of the monodromy operator. These eigenvalues determine the local asymptotic stability of Eq. (1) and the loss of stability according to the criteria shown in Fig. 2. The period can be discretized into a uniform mesh as shown in Fig. 3a,

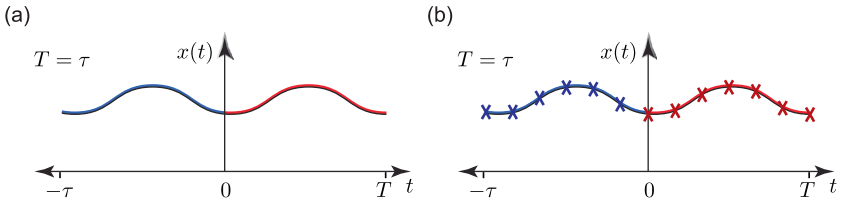

Fig. 1. Mapping of the history segment on $[-\tau,0]$ one period ahead onto $[-\tau+T,T]$. (a) The continuous state-space; whereas (b) a discretization of the state-space.

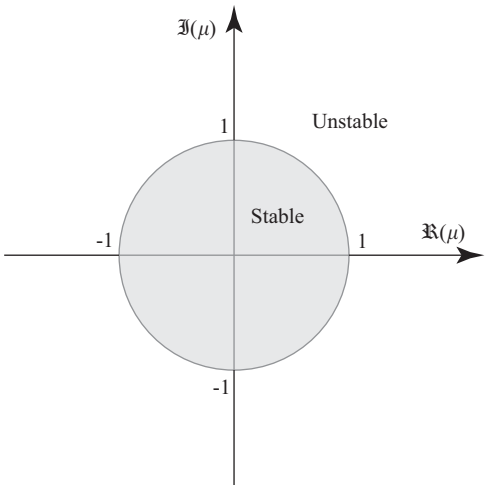

Fig. 2. The stability criteria for the dynamic map in Eq. (2). The system is asymptotically stable if all the eigenvalues of U lie within the unit circle in the complex plane, unit circle shown shaded.

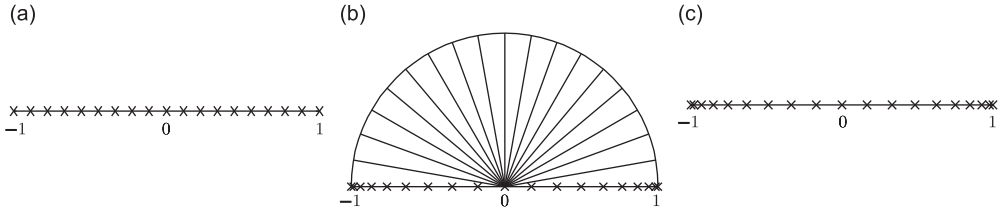

Fig. 3. Some of the common choices for discretization mesh t_i. (a) An equi-spaced grid where $t_i = -1 + ih$ and $h = 2/n$. (b) A Chebyshev grid of the first kind where $t_i = \cos(\pi i/n)$. (c) A Legendre–Gauss–Lobatto (LGL) grid where t_i equals the ith root of $(1-t^2)L_n'(t) = 0$, and $L_n(t)$ is the nth order Legendre polynomial.

or a non-uniform mesh such as the pseudo spectral meshes shown in Fig. 3b and c. Uniform meshes typically have a low order polynomial of fixed degree, and increasing the accuracy of the approximation is accomplished by increasing the number of intervals. Increasing the number of uniform intervals, sometimes referred to as "h-convergence", reduces the error on the order of $O[1/n]$ for a linear convergence where n is the number of intervals [24]. A pseudo spectral mesh however, increases the accuracy of the approximation by increasing the order of polynomial rather than the number of intervals. Increasing the order of polynomial, sometimes referred to as "p-convergence", reduces the error on the order of $O[(1/n)^n]$ for an "exponential" convergence where n is the order of the polynomial [24]. In addition, pseudo spectral meshes can be split into several elements for spectral element methods that have "hp-convergence."

Each method described in this section provides a scheme to obtain a finite dimensional approximation for the infinite dimensional monodromy operator. Specifically, we describe the semi-discretization approach, the spectral element method, and the collocation approach. All the methods are based on discretizing the state-space of Eq. (1) to obtain a monodromy matrix **U**. The eigenvalues obtained from **U** are then used to ascertain the stability of Eq. (1) based on the criteria in Fig. 2.

2.1. Semi-discretization

The semi-discretization approach approximates the DDE using a system of linear, first order, ordinary differential equations (ODEs). This method is capable of solving a wide class of DDEs, including autonomous and non-autonomous equations [21]. To illustrate the basic steps of semi-discretization, consider the general non-autonomous DDE in Eq. (1) where the current states and the delayed states are given by the vectors $\mathbf{x}(t)$ and $\mathbf{x}(t-\tau)$, respectively.

The first step in semi-discretization is to discretize the period T into equal intervals of Δt according to

$$\Delta t = \frac{T}{k}, \tag{3}$$

where k is the number of intervals used. The choice of T is obvious for non-autonomous systems; however, for autonomous systems, the period may be arbitrarily chosen as the duration of the delay $T = \tau$. Another choice for autonomous systems is to use a period of $T = \Delta t = \tau/k$.

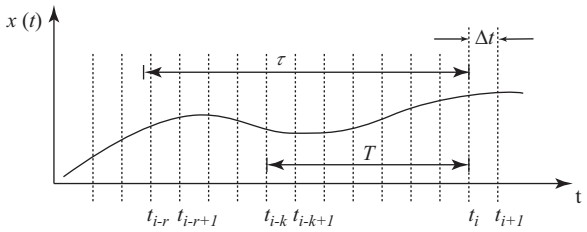

Fig. 4. Semi-discretization intervals for the state x. Note that the intervals are all of equal duration.

Next, we take a closer look at how time is discretized as demonstrated in Fig. 4. Three intervals are highlighted: (1) the current interval between nodes t_i and t_{i+1}, (2) the interval one period prior to the current interval between nodes t_{i-k} and t_{i-k+1}, and (3) the interval nearest to the delay τ between nodes t_{i-r} and t_{i-r+1}. The most general case is shown where the delay is not equal to the period, and the delay can also be shorter than the period.

The delay interval t_{i-r} to t_{i-r+1} is the interval whose beginning is closest to the delay, and the delay interval may or may not contain the beginning of the delay. The delay interval is found by defining r, the beginning of the delay interval, by

$$r = \text{round}\left(\frac{\tau}{\Delta t} + \frac{p}{2} - \frac{1}{2}\right), \tag{4}$$

where p is the order of the semi-discretization. We will consider the first order semi-discretization method in this paper as second and higher orders do not significantly improve convergence properties if the time periodic terms are approximated by piecewise constants [23]. It should be noted that while the first order semi-discretization employs a larger order polynomial than the zeroth order version, the polynomial order remains constant while the number of intervals is increased in order to improve the approximation. Therefore, the semi-discretization method exhibits h-convergence even for the higher order implementations.

If the intervals defined above are small enough, the time-periodic matrix $\mathbf{A}(t)$ can be approximated by the average value over the interval. For example, during the ith interval, $\mathbf{A}(t)$ can be approximated by

$$\mathbf{A}_i = \frac{1}{\Delta t}\int_{t_i}^{t_{i+1}} \mathbf{A}(t)\,\mathrm{d}t, \tag{5}$$

where $\mathbf{A}_i$ is the time average over the interval i for $\mathbf{A}(t)$. Averaging the time dependent coefficient removes the time dependency of $\mathbf{A}$ over the small intervals of duration Δt. Additional linearization is performed by estimating the states $\mathbf{x}$ by a polynomial over the delay interval [23]. This second assumption increases the fidelity of the approximation, and an analytical solution is still available. After applying these small interval assumptions, the DDE is approximated over each interval by a series of linear ODEs of the form

$$\dot{\mathbf{x}}(t) = \mathbf{A}_i\mathbf{x}(t) + \mathbf{B}(t)\mathbf{u}(t), \tag{6}$$

where $\mathbf{u}(t)$ is a polynomial that estimates the value of the states $\mathbf{x}$ over the interval at the delay. For the first order semi-discretization, the polynomial is

$$\mathbf{u}(s) = \left(\frac{s}{\Delta t} - \frac{\tau - r\Delta t}{\Delta t}\right)\mathbf{x}((i-r+1)\Delta t) + \left(\frac{\Delta t - s}{\Delta t} - \frac{\tau - r\Delta t}{\Delta t}\right)\mathbf{x}((i-r)\Delta t), \tag{7}$$

where s is the local time within the delay interval and varies from 0 to Δt. The variable s can be replaced by $t - i\Delta t$ in order to make $\mathbf{u}(s)$ a function of t. This function can be viewed as the sum of two lines as shown in Fig. 5. In this interpretation, the lines have either a positive or negative slope of $1/\Delta t$, and the offsets are weighting factors. In Fig. 5 the weighting factor $\Delta x_{i-r} = -((\tau - r\Delta t)/\Delta t)x((i-r)\Delta t)$ in the first terms of Eq. (7), and $\Delta x_{i-r+1} = -((\tau - r\Delta t)/\Delta t)x((i-r+1)\Delta t)$ in the second term.

The solution of Eq. (6) for any interval can be found [30] as

$$\mathbf{x}(t) = \mathrm{e}^{\mathbf{A}_i(t-t_i)}\mathbf{x}_i + \int_{t_i}^{t} \mathrm{e}^{\mathbf{A}_i(t-s)}\mathbf{B}(s)\mathbf{u}(s)\,\mathrm{d}s, \tag{8}$$

where s is the local time within the interval, t_i is the time at the beginning of the interval, $\mathbf{x}_i$ is the value of the states at t_i, and $\mathbf{u}(s)$ is the approximated state from Eq. (7). The solution is valid inside of the entire interval, but we are interested in the values of the state at the end of the interval so that we can map states from the beginning of the interval to its end. If the matrix $\mathbf{B}$ is constant, then Eq. (8) can be integrated analytically for the values of $\mathbf{x}$ at the end of the interval. The resulting solution is given by

$$\mathbf{x}_{i+1} = \mathrm{e}^{\mathbf{A}_i\Delta t}\mathbf{x}_i + \mathbf{R}_{i,1}\mathbf{x}_{i-r+1} + \mathbf{R}_{i,0}\mathbf{x}_{i-r}, \tag{9a}$$

$$\mathbf{R}_{i,1} = \mathbf{B}\left(-\mathbf{A}_i^{-1} + \frac{1}{\Delta t}(-\mathbf{A}_i^{-2} + (\tau - r\Delta t)\mathbf{A}_i^{-1})\right)(\mathbf{I} - \mathrm{e}^{\mathbf{A}_i\Delta t}), \tag{9b}$$

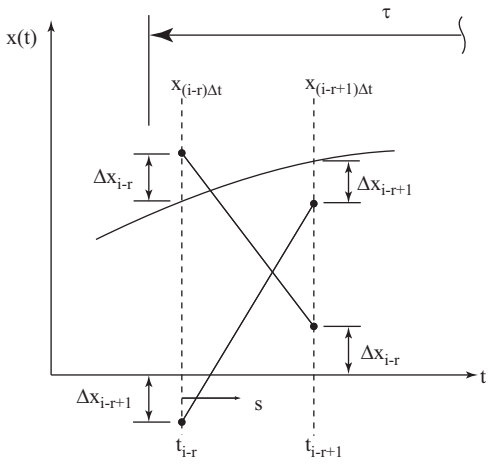

Fig. 5. Linear estimation of the state x in the delay interval for the first-order semi-discretization. The weighting factor $\Delta x_{i-r} = -((\tau - r\Delta t)/\Delta t)x_{(i-r)\Delta t}$ and $\Delta x_{i-r+1} = -((\tau - r\Delta t)/\Delta t)x_{(i-r+1)\Delta t}$. The local time s is zero at t_{i-r} and equal to Δt at t_{i-r+1}.

$$\mathbf{R}_{i,0} = \mathbf{B}\left(\mathbf{A}_i^{-1} + \frac{1}{\Delta t}(\mathbf{A}_i^{-2} - (\tau - (r-1)\Delta t)\mathbf{A}_i^{-1})\right)(\mathbf{I} - e^{\mathbf{A}_i \Delta t}), \tag{9c}$$

where $\mathbf{I}$ is the identity matrix, and Δt has replaced $t_{i+1} - t_i$ [23]. The solution is only valid if the inverse of $\mathbf{A}$ exists. For the zeroth order semi-discretization, the state $\mathbf{x}$ during the delay interval is a constant, estimated by the value of the state at the delay x_{i-r}. The resulting value for $\mathbf{R}_{i,1}$ is zero and $\mathbf{R}_{i,0} = \mathbf{B}(e^{\mathbf{A}_i \Delta t} - \mathbf{I})\mathbf{A}_i^{-1}$ for the zeroth order case and a constant $\mathbf{B}$ [23].

The next step is to systematically construct a discrete map for each interval, mapping the values at the beginning of each interval to its end. This relationship is defined by

$$\mathbf{x}_{i+1} = \mathbf{M}_i \mathbf{x}_i, \tag{10}$$

where $\mathbf{x}_{i+1}$ is a column vector of the states at the end of each interval and $\mathbf{x}_i$ is a column vector of the states at the beginning of each interval. The matrix $\mathbf{M}_i$ maps the states at the beginning of the interval to the states at the end of the interval and can be written out as

$$\mathbf{M}_i = \begin{bmatrix} e^{\mathbf{A}_i \Delta t} & 0 & \cdots & \mathbf{R}_{i,1} & \mathbf{R}_{i,0} \\ \mathbf{I} & 0 & \cdots & 0 & 0 \\ 0 & \mathbf{I} & \cdots & 0 & 0 \\ \vdots & \vdots & \ddots & \vdots & \vdots \\ 0 & 0 & \cdots & \mathbf{I} & 0 \end{bmatrix}. \tag{11}$$

As can be seen in Eq. (11), the top row enforces the relationship between $\mathbf{x}_{i+1}$ and $\mathbf{x}_i$ defined in Eq. (9a). The remainder of the matrix equates like terms from vectors $\mathbf{x}_{i+1}$ and $\mathbf{x}_i$. The size of the matrix $\mathbf{M}_i$ is determined by the variable r and the degree of freedom of the system of delay equations.

Finally, using the relationship $\mathbf{M}_i$ between the beginning and the end of each interval, the relationship between the beginning and end of the period may be calculated. This is accomplished by multiplying the mapping matrix $\mathbf{M}_i$ of each interval from the beginning of the period to its end [22] as shown by

$$\mathbf{x}_{k+1} = \mathbf{M}_{r-1}\mathbf{M}_{r-2} \ldots \mathbf{M}_0 \mathbf{x}_k = \mathbf{U}\mathbf{x}_k. \tag{12}$$

The resulting product is the monodromy matrix $\mathbf{U}$. The eigenvalues of the monodromy matrix $\mathbf{U}$, also known as the characteristic multipliers, indicate the stability of the system.

2.2. Spectral element

The spectral element method approximates the solution to DDEs based on the method of weighted residuals. In the spectral element method, the time-line is discretized with nodes as shown in Fig. 6. In the most general case, the spectral element method may include multiple elements in each period for *hp*-convergence. However, for simplicity, the following explanation will assume one element per period for *p*-convergence. Note that increasing the number of nodes leads to significantly quicker convergence than increasing the number of elements, so for most cases there is no loss of performance due to this simplification.

We will use Legendre–Gauss–Lobatto (LGL) points for the spectral element implementation in this paper, but Chebyshev points could be used instead. The LGL points create a non-uniform mesh which allows a large number of nodes to be used in each period. If equi-distributed points were used instead, increasing the number of nodes would lead to ill-conditioned systems, especially for the meshes of eight or more nodes [31]. The LGL nodes are computed from the roots of the polynomial

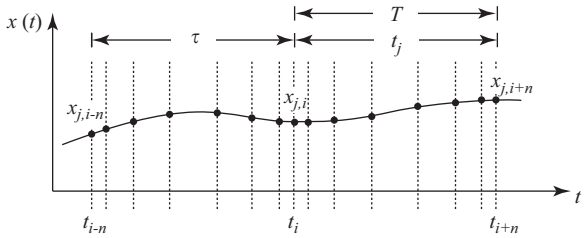

Fig. 6. Spectral element mesh for the state x. Note that the mesh is non-uniform.

$(1-u^2)L_n'(u)$ where $L_n(u)$ is the nth order Legendre function, $L_n'(u)$ is the first derivative of $L_n(u)$ with respect to u, and u ranges between -1 and 1. The LGL nodes must be shifted to the arbitrary interval $[a,b]$ of the period through the relation

$$\tilde{u} = \frac{b-a}{2}u + \frac{b+a}{2}, \tag{13}$$

where $u \in [-1,1]$ and $\tilde{u} \in [a,b]$.

The solution is approximated at each grid point using polynomial trial functions for each period according to

$$\mathbf{x}_j(t) = \sum_{i=1}^{n+1} \mathbf{x}_{j,i}\phi_i(\eta), \tag{14a}$$

$$\mathbf{x}_j(t-\tau) = \sum_{i=1}^{n+1} \mathbf{x}_{j,i-n}\phi_i(\eta), \tag{14b}$$

where $\mathbf{x}_{j,i}(t)$ is the vector of discretized states of the element j, $\phi_i(\eta)$ is the trial function, and η is the normalized local time for each element. The normalized local time η is defined as $\eta = \sigma/t_j$ where σ is the local coordinate of the element j, and t_j is the duration of the element.

The trial functions ϕ_i can be found using the barycentric Lagrange formula

$$\phi_i(t) = \frac{\dfrac{\rho_i}{t-t_i}}{\sum_{j=1}^{n+1}\dfrac{\rho_j}{t-t_j}}, \tag{15}$$

and the barycentric weights are given by

$$\rho_i = \frac{1}{\prod_{k=1,k\neq i}^{n+1}(t_i-t_k)}, \quad k = 1,2,\ldots,n+1. \tag{16}$$

Computing $\phi_i(t)$ only requires the mesh information. In this paper, we used a barycentric form of the Lagrange representation. The effect of rounding errors, which is directly related to the stability of the formula, has been discussed in Higham [32]. To summarize the results of Higham, the barycentric formula is numerically stable if a good set of interpolation points is chosen. Specifically, error bounds grow slowly as the number of interpolation points (order of the interpolating polynomial) is increased. Since we used the Legendre–Gauss–Lobatto points, which constitute a set with good interpolation properties, the error grows slowly with the degree of the polynomial. Our calculations used the standard unit roundoff of floating point arithmetic in Matlab which is approximately equal to 10^{-16}.

The trial functions obtained from Eq. (15) have two useful properties. First, they are independent of the data or the function being approximated. This means that once the trial functions are obtained for a certain mesh, they can be reused to approximate any continuous function on the same mesh. Second, at the ith mesh point, the ith trial function is equal to unity, whereas all the other trial functions are equal to zero. This is expressed by the equation

$$\phi_i(t_k) = \delta_{i,k}, \quad t_k \in \{t_i\}_{i=1}^{n+1}, \tag{17}$$

where δ is the Kronecker delta. The barycentric formula can also be used to obtain the derivative of the trial functions at the interpolation nodes according to

$$\phi_i'(t_k) = \begin{cases} \dfrac{\rho_i/\rho_k}{t_i-t_k}, & i \neq k, \\ \displaystyle\sum_{i=0,i\neq k}^{n+1} \frac{-\rho_i/\rho_k}{t_i-t_k}, & i = k. \end{cases} \tag{18}$$

Eq. (18) is useful for approximating the derivatives of the states at the mesh point. For example, assume that the vector of states is given by $\mathbf{z}$. Then, if the barycentric Lagrange formula is used to approximate $\mathbf{z}$ on a mesh $\{t_i\}$, then the derivative $\mathbf{z}'$

on $\{t_i\}$ is given by

$$\mathbf{z}' = \mathbf{D}\mathbf{z}, \tag{19}$$

where $D_{ki} = \phi_i'(t_k)$.

The approximation of the continuous states $\mathbf{x}(t)$ is made up of the coefficients $\mathbf{x}_{j,i}$ (the values of $\mathbf{x}(t)$ at the nodes) and the trial functions $\phi_i(\eta)$. The indices i and j refer to the node and element, respectively. Substituting the approximate solution into Eq. (1) gives

$$\sum_{i=1}^{n+1}\left(\frac{1}{t_j}\mathbf{x}_{j,i}\phi_i'(\eta) - \mathbf{A}(t_\eta)\mathbf{x}_{j,i}\phi_i(\eta) - \mathbf{B}(t_\eta)\mathbf{x}_{j,i-n}\phi_i(\eta)\right) = \text{error}, \tag{20}$$

where $t_\eta = (\eta + j - 1)t_j$, the prime indicates a derivative with respect to η, and the error term is associated with the approximation procedure.

The approximation error in Eq. (20) can be minimized by multiplying the approximate solution by a set of independent test functions and setting the integral over the duration of the element equal to zero. This is called the method of weighted residuals which also generates enough equations to create the dynamic map [33]. The spectral element method uses Legendre polynomials for the test functions. Further, to keep the resulting matrices square, the number of the test functions is always one less than the number of the trial functions. Assuming that the index of the test functions $\psi(\eta)$ is p, the weighted expression of Eq. (20) becomes

$$\int_0^1 \left(\frac{1}{t_j}\mathbf{x}_{j,i}\phi_i'(\eta) - \mathbf{A}(t_\eta)\mathbf{x}_{j,i}\phi_i(\eta) - \mathbf{B}(t_\eta)\mathbf{x}_{j,i-n}\phi_i(\eta)\right)\psi_p(\eta)\,\mathrm{d}\eta = 0. \tag{21}$$

Applying each test function in turn, the resulting equations for each element can be combined into a global matrix equation. The resulting expression for the global matrix with one element for each period and $n+1$ nodes is

$$\begin{bmatrix} \mathbf{I} & 0 & \cdots & 0 & 0 \\ \mathbf{N}_{j,i}^1 & \mathbf{N}_{j,i+1}^1 & \cdots & \mathbf{N}_{j,i+n-1}^1 & \mathbf{N}_{j,i+n}^1 \\ \mathbf{N}_{j,i}^2 & \mathbf{N}_{j,i+1}^2 & \cdots & \mathbf{N}_{j,i+n-1}^2 & \mathbf{N}_{j,i+n}^2 \\ \vdots & \vdots & \ddots & \vdots & \vdots \\ \mathbf{N}_{j,i}^n & \mathbf{N}_{j,i+1}^n & \cdots & \mathbf{N}_{j,i+n-1}^n & \mathbf{N}_{j,i+n}^n \end{bmatrix} \begin{bmatrix} \mathbf{x}_{j,i} \\ \mathbf{x}_{j,i+1} \\ \vdots \\ \mathbf{x}_{j,i+n-1} \\ \mathbf{x}_{j,i+n} \end{bmatrix} = \begin{bmatrix} 0 & 0 & \cdots & 0 & \mathbf{I} \\ \mathbf{P}_{j,i-n}^1 & \mathbf{P}_{j,i-n+1}^1 & \cdots & \mathbf{P}_{j,i-1}^1 & \mathbf{P}_{j,i}^1 \\ \mathbf{P}_{j,i-n}^2 & \mathbf{P}_{j,i-n+1}^2 & \cdots & \mathbf{P}_{j,i-1}^2 & \mathbf{P}_{j,i}^2 \\ \vdots & \vdots & \ddots & \vdots & \vdots \\ \mathbf{P}_{j,i-n}^n & \mathbf{P}_{j,i-n+1}^n & \cdots & \mathbf{P}_{j,i-1}^n & \mathbf{P}_{j,i}^n \end{bmatrix} \begin{bmatrix} \mathbf{x}_{j,i-n} \\ \mathbf{x}_{j,i-n+1} \\ \vdots \\ \mathbf{x}_{j,i-1} \\ \mathbf{x}_{j,i} \end{bmatrix}, \tag{22}$$

where $\mathbf{I}$ is the $d \times d$ identity matrix. The expressions for the matrices $\mathbf{N}$ and $\mathbf{P}$ populating the global matrices are

$$\mathbf{N}_{ji}^p = \int_0^1 \left(\frac{1}{t_j}\mathbf{I}\phi_i'(\eta) - \mathbf{A}(t_\eta)\phi_i(\eta)\right)\psi_p(\eta)\,\mathrm{d}\eta, \tag{23a}$$

$$\mathbf{P}_{ji}^p = \int_0^1 \mathbf{B}(t_\eta)\phi_i(\eta)\psi_p(\eta)\,\mathrm{d}\eta, \tag{23b}$$

where both matrices are of dimension $d \times d$.

The integrals in Eq. (23) are integrated using a LGL quadrature which estimates an integral by replacing it with a weighted summation of the function values at the LGL points. Denoting the integrand resulting from the weighted residual method by $f(\eta)$, the corresponding expression for the LGL quadrature is

$$\int_0^1 f(\eta)\,\mathrm{d}\eta \approx \sum_{k=1}^{n+1} w_k f(\eta_k), \tag{24}$$

where η_k are the Legendre points shifted from the interval $[-1, 1]$ to $[0, 1]$ using Eq. (13), $f(\eta_k)$ are the values of $f(\eta)$ evaluated at the LGL points [34], and w_k are the LGL quadrature weights given by the equation

$$w_k = \begin{cases} \dfrac{2}{n(n+1)} & k = 1, n+1, \\ \dfrac{2}{n(n+1)(L_n(\eta_k))^2} & \text{otherwise}. \end{cases} \tag{25}$$

Eqs. (24) and (25) are used to evaluate the integrals in Eq. (23) which are then used to populate the corresponding global matrices. Applying the LGL quadrature rule to these integrals and using the properties of the trial functions yields

$$\mathbf{N}_{ji}^p = \sum_{k=1}^{n+1}\left(\frac{1}{t_j}\mathbf{I}\phi_i'(\eta_k)\psi_p(\eta_k)w_k\right) - \mathbf{A}(t_\eta)\psi_p(\eta_i)w_i, \tag{26a}$$

$$\mathbf{P}_{ji}^p = \mathbf{B}(t_\eta)\psi_p(\eta_i)w_i. \tag{26b}$$

Eq. (22) can be used to define a dynamic map that has the same form as Eq. (2). This map is given by

$$\mathbf{H}\mathbf{x}_k = \mathbf{G}\mathbf{x}_{k-1}, \tag{27}$$

where the subscripts k and $k-1$ refer to the current and the previous periods, respectively. The monodromy matrix can be calculated by $\mathbf{U}=\mathbf{H}^{-1}\mathbf{G}$, and the stability of this system can be determined by the eigenvalues of $\mathbf{U}$.

2.3. Legendre collocation method

The Legendre collocation method is a weighted residual method similar to the spectral element method [24]. In the Legendre collocation method, the time-line is discretized with nodes as shown in Fig. 7. While the spectral element method minimizes the error element-wise, the Legendre collocation method minimizes the error point-wise. The Legendre collocation method uses the same LGL mesh, trial functions ϕ_i of Eq. (15), and trial function derivatives ϕ_i' of Eq. (18) as the spectral element method. To demonstrate the difference between the Legendre collocation method and the spectral element method, consider again Eq. (21). The key difference between the two methods is the choice of the test functions $\psi_p(\eta)$. The test functions in the Legendre collocation method are the Dirac delta functions at the mesh nodes. These functions are described by

$$\{\psi_p(\eta)\}_{p=1}^{N}=\{\delta(\eta-\eta_p)\}_{p=1}^{N}, \tag{28}$$

where $\{\eta_p\}$ is the set of collocation points and $\delta(\eta-\eta_p)$ is the Dirac delta function. In this paper we will use LGL points for the collocation points, but it is possible to use Chebyshev points instead. Therefore, by examining Eq. (21) for this choice of ψ_p, it becomes clear that the collocation approach requires the DDE to be satisfied at the set of mesh nodes. Specifically, using the collocation approach on Eq. (1) gives

$$\hat{\mathbf{D}}\mathbf{x}_k=\hat{\mathbf{M}}_A\mathbf{x}_k+\hat{\mathbf{M}}_B\mathbf{x}_{k-1}, \tag{29}$$

where $\mathbf{x}_k$ contains the values of the states in the present period, and $\mathbf{x}_{k-1}$ contains the values of the states in the previous period. $\hat{\mathbf{M}}_A$ is a $q(N+1)$ matrix with entries

$$\hat{\mathbf{M}}_A=\begin{bmatrix}\mathbf{A}(t_0) & 0_q & \cdots & & 0_q\\ 0_q & \mathbf{A}(t_1) & & & \vdots\\ \vdots & & \ddots & & \\ & & & \mathbf{A}(t_{N-1}) & 0_q\\ 0_q & \cdots & & 0_q & 0_q\end{bmatrix}, \tag{30}$$

where $\mathbf{A}(t_i)$ is the value of $\mathbf{A}(t)$ evaluated at the ith collocation point. Similarly, $\hat{\mathbf{M}}_B$ has the entries

$$\hat{\mathbf{M}}_B=\begin{bmatrix}\mathbf{B}(t_0) & 0_q & \cdots & & 0_q\\ 0_q & \mathbf{B}(t_1) & & & \vdots\\ \vdots & & \ddots & & \\ & & & \mathbf{B}(t_{N-1}) & 0_q\\ 0_q & \cdots & & 0_q & \mathbf{I}_q\end{bmatrix}. \tag{31}$$

The matrix $\hat{\mathbf{D}}$ is calculated from the matrix $\mathbf{D}$ in Eq. (19). $\mathbf{D}$ is first shifted to the interval $[a,b]$ with the scaling factor $2/(b-a)$. The spectral differentiation matrix, which is defined as the Kronecker product $\mathbb{D}=\mathbf{D}\otimes\mathbf{I}_q$, is then calculated using the shifted $\mathbf{D}$. $\hat{\mathbf{D}}$ is a modified version of the spectral differentiation matrix $\mathbb{D}$, that is multiplied by $2/\tau$ to shift to the interval $[0,\tau]$, and the last q rows are changed to $[\mathbf{I}_q 0_q \ldots 0_q]$. The change in the last q rows serves to enforce the continuity condition that the states are equal at the end of one period and the beginning of the next.

Eq. (29) can be rewritten in the form $\mathbf{x}_k=\mathbf{U}\mathbf{x}_{k-1}$, where $\mathbf{U}$ is the monodromy matrix given by $\mathbf{U}=(\hat{\mathbf{D}}-\hat{\mathbf{M}}_A)^{-1}\hat{\mathbf{M}}_B$. Eq. (28) reveals that the collocation method is a special case of the weighted residual approach. Since spectral element and collocation methods adopt different strategies to reduce the error, the test functions used in Eq. (21) define the resulting analysis technique.

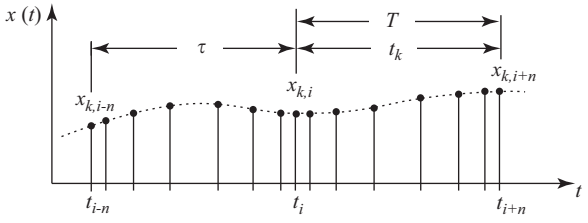

Fig. 7. Legendre collocation element mesh for the state x. Note that the mesh is non-uniform.

3. Criteria for comparison

In this paper we are interested in comparing the performance of each method in generating stability diagrams of DDE systems. Generating such a diagram, especially at the border of stable and unstable regions, requires a good approximation of the maximum eigenvalue of the monodromy operator in a reasonable amount of computational time. Therefore, the criteria of comparison used in this paper are the convergence of the maximum eigenvalues and the computational time required to generate a converged stability diagram for each method.

To reach convergence, the calculated eigenvalues must approach the largest eigenvalues of the monodromy operator as the finite divisions of the period are reduced. The smallest monodromy matrix required to accurately estimate the monodromy operator is directly proportional to the computational dimension of each method which is the number of collocation points in the Legendre collocation method, the number of intervals in the semi-discretization method, and the number of mesh points in the spectral element method. Only one element is used for both the Legendre collocation and spectral element methods. In the following numerical studies, the computational dimension was increased from three to $N_{\max}=50$ for each method. For each computational dimension, we calculated the approximate maximum eigenvalue for one point on the stability diagram. The error measure used for the convergence is the absolute error

$$\epsilon_{\text{stability}}=|\lambda-\mu^*|, \tag{32}$$

where $\lambda=\max|\mu|$ is the approximation of the maximum eigenvalue, whereas μ^* is the reference maximum eigenvalue obtained with the Legendre collocation approach ($\mu^*=\max(|\mu(N_{\max})|)$). The absolute error is plotted as a function of the computational dimension, and the rate at which each method approaches convergence is compared. In the following studies, convergence is defined as the computational dimension at which the absolute error calculated by Eq. (32) is zero within the standard unit roundoff of floating point arithmetic in Matlab which is approximately equal to 10^{-16}.

To compare the computational time of each method, we measured the time required to calculate the converged stability diagram five times for each numerical study and recorded the average. For each method, we used the smallest computational dimension required to achieve convergence which is equivalent to the smallest monodromy matrix required. All three methods were programmed as their "full" algorithm and in the same basic code structure. No computational tricks or optimization techniques were used in order to provide the best comparison. We also compared our implementation of zeroth order semi-discretization with the zeroth order code provided by Insperger [22] (we made small changes to Insperger's code such as using matrix division instead of "inv" and initializing vectors). The code provided by Insperger includes matrix truncation, but we found the average computation time of 271.1 s to be nearly identical to the average of 273.6 s required by our code for identical parameters. Since all three methods can be improved by various techniques, we feel that the comparisons provided in this paper are fair and accurate. In addition, the computational times reported are intended for a comparison of the efficiency of each method and not as an absolute measure. It is expected that advances in computer technology will increase the computational speeds of each method, but will not significantly change the relative speed between methods. Each method was programmed in Matlab R2010b and run on a Windows 7 PC with an Intel(R) Core(TM) i5 CPU @2.26 GHz with 4 GB of installed memory.

4. Numerical studies

In this section, we present numerical studies for a ship stability model, the delayed damped Mathieu equation, and a helicopter rotor control stability problem. For all three studies, we present a brief description of the physical representation, the key parameters, and the $\mathbf{A}(t)$ and $\mathbf{B}(t)$ state space matrices for Eq. (1). We then present the results of the numerical comparisons for the three methods. These results include stability diagrams of the systems, convergence plots, and tables comparing the computational performance.

4.1. Ship stability

Ships can be stabilized by the "activated tanks method" where a ballast is displaced between tanks by means of an axial propeller pump. The pump is controlled by instruments responsive to the ship's angular motion. The phase of the moving ballast is such that the ballast concentration is at a maximum in a tank which rises in space (due to rolling) when the angular velocity is also a maximum. When the pump begins to work beyond its capacity, the resulting cavitation results in a delayed damping term and the following delay differential equation:

$$\ddot{x}(t)+k\dot{x}(t)+K\dot{x}(t-\tau)+\omega_0^2x(t)=a\sin\omega t, \tag{33}$$

where x is the roll motion, and K is the damping associated with the stabilizing equipment [35,36]. A variational equation can be obtained from Eq. (33) by substituting $x=x_p+\xi(t)$ and subtracting the periodic motion x_p. Non-dimensionalizing this equation we have

$$\xi''(\eta)+\alpha\xi'(\eta)+\beta\xi'(\eta-\hat{\tau})+\xi(\eta)=0, \tag{34}$$

where η is dimensionless time ($\eta=\omega_0 t$), $\hat{\tau}$ is a dimensionless delay, a prime represents a derivative with respect to η, $\alpha=k/\omega_0$, and $\beta=K/\omega_0$ [36]. The state space matrices **A** and **B** are given by

$$\mathbf{A}=\begin{bmatrix}0 & 1\\ -1 & -\alpha\end{bmatrix},\quad \mathbf{B}=\begin{bmatrix}0 & 0\\ 0 & -\beta\end{bmatrix}. \tag{35}$$

The stability diagram for this system is shown in Fig. 8a with a 100×100 grid in α, β parameter space. The stability diagram was generated using each method with nearly identical results. The semi-discretization method generated a diagram that had a slightly larger stable region than the other two methods. The stability diagram shown was created with the spectral element method using 12 mesh points.

The convergence plot shown in Fig. 8b was created using the point $(\alpha,\beta)=(20,20)$ which is in the stable region. We selected this point due to its sensitivity to convergence and its proximity to the stability border. The results are summarized in Table 1 with the spectral element method converging with the smallest computational dimension of 12 mesh points. The semi-discretization method, however, does not converge when using less than 50 intervals or even up to 200 intervals. We fitted a line to the absolute error of the semi-discretization method using least squares and found that more than 1×10^7 intervals are required for convergence. The convergence rate of both the zeroth and first-order semi-discretization methods is compared in Fig. 9. While the first-order method does have slightly improved convergence properties over the zeroth method, both clearly converge linearly.

The results of the relative computational time comparison are summarized in Table 1 with the Legendre collocation method requiring the least amount of time at 12.0 s. Since the semi-discretization method does not converge when using less than 50 intervals in this case, any choice of intervals less than 50 would be arbitrary. We selected 21 intervals which is the same number of collocation points required by the Legendre collocation method to converge.

4.2. Delayed damped Mathieu equation

The delayed damped Mathieu equation (DDME) is an adaptation of the original equation proposed by Mathieu in the study of elliptical membranes [25]. The DDME has become a standard equation for comparing and evaluating delay methods. The equation in its full form of

$$\ddot{x}(t)+\kappa\dot{x}(t)+\left(\delta+\epsilon\cos\left(\frac{2\pi t}{T}\right)\right)x(t)=bx(t-\tau), \tag{36}$$

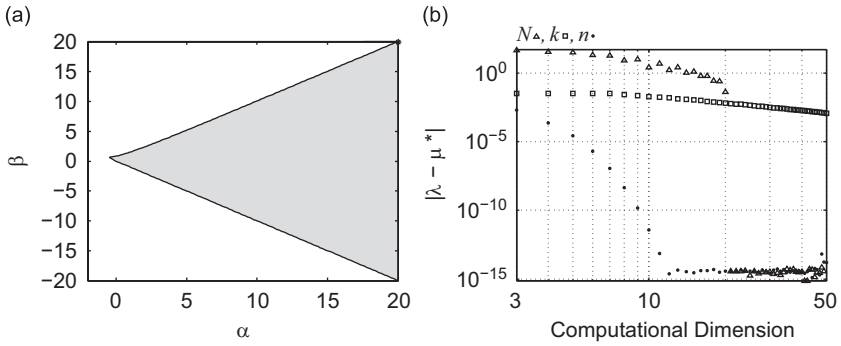

Fig. 8. The stability diagram for Eq. (34) and the convergence plots for the point $(\alpha,\beta)=(20,20)$. In graph (a) the stable regions are shaded, the unstable regions are left unshaded, and the point used for the convergence is indicated with a star. Graph (b) shows the convergence of the maximum eigenvalue as a function of the computational dimension of (1) the Legendre collocation method (triangles), (2) the semi-discretization method (squares), and (3) the spectral element method (dots).

Table 1
For the ship stability in Eq. (34), the minimum computational dimension required to achieve convergence and the computational time required to calculate the stability diagram is summarized.

Method	Computational dimension	Computational time (s)
Semi-discretization	21+	47.1
Spectral element	12	15.6
Legendre collocation	21	12.0

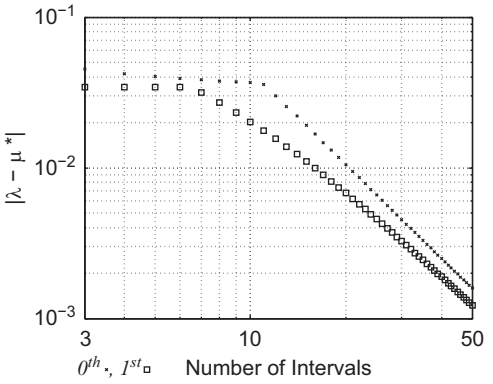

Fig. 9. Convergence plot for the point $(\alpha,\beta)=(20,20)$ comparing the zeroth and first-order semi-discretization methods. The graph shows the convergence of the maximum eigenvalue as a function of the computational dimension of (1) the zeroth-order semi-discretization method (*x*s) and (2) the first-order semi-discretization method (squares). Notice both methods show linear convergence rate, but neither method reaches convergence in the plot (convergence occurs at about 1×10^{-15}).

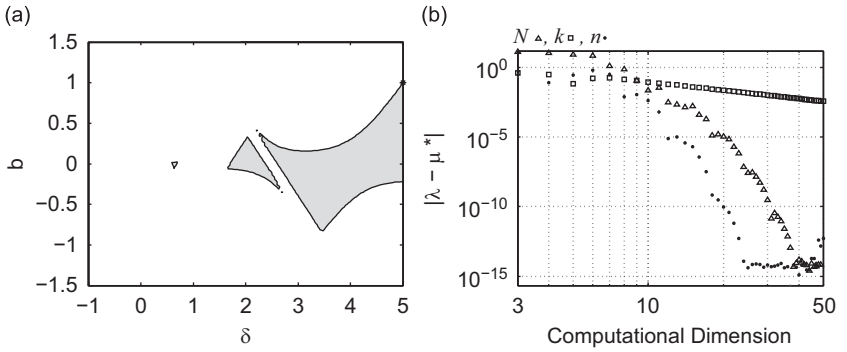

Fig. 10. The stability diagram for Eq. (36) and the convergence plots for the point $(\delta,b)=(5,1)$. In graph (a) the stable regions are shaded, the unstable regions are left unshaded, and the point used for the convergence is indicated with a star. Graph (b) shows the convergence of the maximum eigenvalue as a function of the computational dimension of (1) the Legendre collocation method (triangles), (2) the semi-discretization method (squares), and (3) the spectral element method (dots).

is a second order, linear, non-autonomous, single-delayed differential equation. The state space matrices, $\mathbf{A}(t)$ and $\mathbf{B}(t)$, for the DDME are given by

$$\mathbf{A}=\begin{bmatrix} 0 & 1 \\ -\left(\delta+\epsilon\cos\left(\dfrac{2\pi t}{T}\right)\right) & -\kappa \end{bmatrix},\quad \mathbf{B}=\begin{bmatrix} 0 & 0 \\ b & 0 \end{bmatrix}. \tag{37}$$

The DDME is commonly used because it contains many of the intricacies faced by delayed methods in a concise form. In addition, closed form stability charts are available for the DDME which makes it attractive for validating numerical methods [37,38].

The DDME can be viewed as a more complex form of a simple oscillator. From this point of view, κ represents the damping coefficient, and δ represents the stiffness coefficient. The additional term $\epsilon\cos(2\pi t/T)$ represents a periodic fluctuation of the stiffness coefficient with a period of T. The final delay term $bx(t-\tau)$ can be viewed as delayed feedback or hysteresis. In the following comparisons we include a damping coefficient κ of 0.1, a delay τ and period T of 2π, and an amplitude ϵ of 2.

The stability diagram for this system is shown in Fig. 10a with a 100×100 grid in δ, b parameter space. The stability plot was generated using each method with nearly identical results. The stability plot shown was created with the spectral element method using 24 mesh points.

The convergence plot shown in Fig. 10b was created using the point $(\delta,b)=(5,1)$. We selected this point due to its proximity to the stability border. The results are summarized in Table 2 with the spectral method converging with the smallest computational dimension of 24 mesh points. The semi-discretization method does not converge when using less than 50 intervals or even up to 200 intervals. The results of the relative computational time comparison are summarized in Table 2 with the Legendre collocation method requiring the least amount of time at 44.6 s. Since the semi-discretization

Table 2
For the DDME in Eq. (36), the minimum computational dimension required to achieve convergence and the computational time required to calculate the stability diagram is summarized.

Method	Computational dimension	Computational time (s)
Semi-discretization	38+	123.0
Spectral element	24	68.3
Legendre collocation	38	44.6

method does not converge with fewer than 50 intervals, we selected the same number of intervals (38) as collocation points used by the Legendre collocation method.

4.3. Helicopter rotor

Time periodic equations are used to model the flapping of an individual rotor blade in the forward motion of helicopters, and several studies have investigated the stability of helicopter blades in forward motion. The focus in these studies was on designing a control scheme that would attenuate the vibrations (flapping) of the rotor blade. The attenuation of these vibrations improves the ride comfort, reduces fatigue in the rotor, and protects the aircraft's equipment from damage [39].

One control strategy is to control the rotor using measurements obtained from each rotor blade individually. For example, Pandyian and Sinha used Liapunov–Floquet transformation to design an algorithm that controlled the helicopter's individual blade flapping motion [40]. Arcara et al. designed an individual blade control framework based on the measurements of the acceleration, or the vibratory loads each blade transmits to the rotor hub, taken at various locations on each blade [39].

In this study, we explore a delay feedback strategy as a possible alternative for controlling flapping in helicopter blades based on the model in Ref. [40]. However, instead of using the blade pitch as the control input, we introduce a control term based on the flapping of the blade on the previous rotor revolution. The resulting variational equation for the flapping of the rotor blade with a delayed feedback is

$$\dot{\theta}(t) = \mathbf{A}(t)\theta(t) + \mathbf{B}(t)\theta(t-T), \tag{38}$$

where the over dot denotes a differentiation with respect to time, $\theta(t)$ is the flapping of the rotor blade about the periodic solution, and $T=1$ is the period of one rotor revolution. The matrix $\mathbf{A}(t)$ is the system matrix while $\mathbf{B}(t)$ is the matrix of gains associated with the delayed feedback term. The elements of the matrices $\mathbf{A}(t)$ and $\mathbf{B}(t)$ can be written as

$$\mathbf{A} = \begin{bmatrix} 0 & 1 \\ -(2\pi)^2\{1+\omega_F^2+\gamma\left(\frac{\mu}{6}\cos 2\pi t + \frac{\mu^2}{8}\sin 4\pi t\right)\} & -2\pi\gamma\left(\frac{1}{8}+\frac{\mu}{6}\sin 2\pi t\right) \end{bmatrix},$$

$$\mathbf{B} = \begin{bmatrix} 0 & 0 \\ c_1 & c_2 \end{bmatrix}, \tag{39}$$

where ω_F is the non-rotating flap frequency, γ is the Lock number (the ratio of the aerodynamic forces to inertia forces in the blade), μ is the rotor advance ratio of the forward speed to the rotor tip speed, and c_1 and c_2 are the gains for the feedback control signal. Following Ref. [40], the design parameters are $\omega_F = 0.4$ rad/s, $\gamma = 5$, and $\mu = \{0.3, 0.75, 1.2\}$. The stability of the system is studied in the gains parameter space (c_1, c_2).

The stability diagrams for this system are shown in Fig. 11a, c, and e with a 100×100 grid in $c1$, $c2$ parameter space for all three plots. The stability plot was generated using each method with nearly identical results. The semi-discretization method generated a diagram that had a slightly smaller stable region than the other two methods. The stability plots shown were created with the spectral element method using 20, 27, and 29 mesh points for $\mu = 0.3$, $\mu = 0.75$, $\mu = 1.2$, respectively.

The convergence plots shown in Fig. 11b, d, and f were created using the points $(c1, c2) = (0, 4.25)$, $(c1, c2) = (0, 3)$, and $(c1, c2) = (0, 1)$, respectively. We selected these points due to their proximity to the stability border. In Fig. 11f, collocation points were plotted up to 60 to demonstrate convergence more clearly. The spectral method converges with the smallest computational dimension for each set of parameters as summarized in Table 3. The semi-discretization method, however, does not converge with fewer than 50 intervals or even up to 200 intervals for any of the values of μ.

The results of the relative computational time comparison are summarized in Table 3. For each set of parameters, the Legendre collocation method requires the least amount of time. Since the semi-discretization method does not converge when using less than 50 intervals, we selected the same number of collocation points required by the Legendre collocation method to reach convergence.

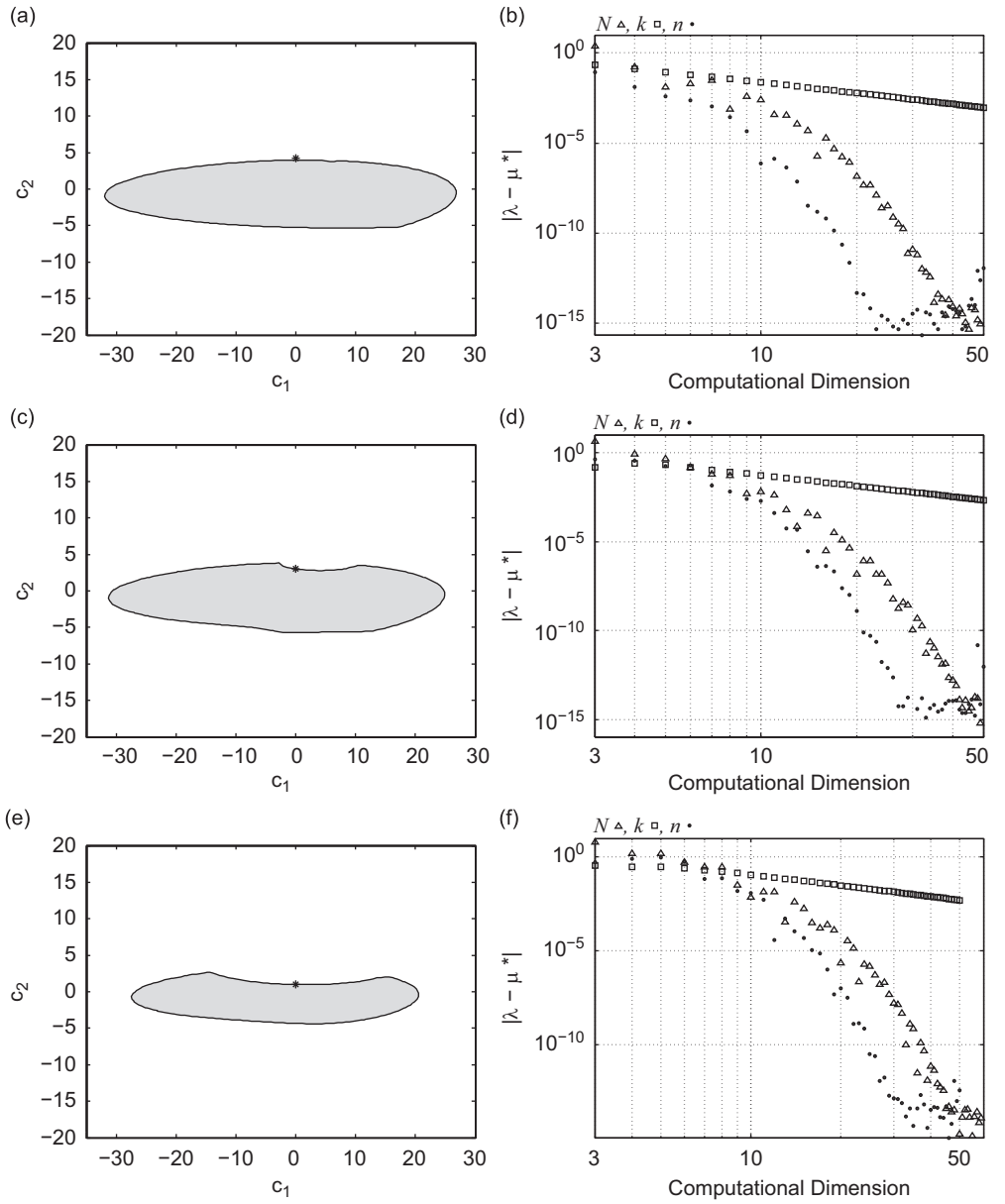

Fig. 11. The stability diagrams for Eq. (38) with $\mu=0.3$ (a), $\mu=0.75$ (c), and $\mu=1.2$ (e). The convergence plots for the (c_1,c_2) points are (0,4.25) for $\mu=0.3$ (b), (0,3.0) for $\mu=0.75$ (d), and (0,1.0) for $\mu=1.2$ (f). In graphs (a), (c), and (e) the stable regions are shaded, the unstable regions are left unshaded, and the point used for the convergence is indicated with a star. Graphs (b), (d), and (f) show the convergence of the maximum eigenvalue as a function of (1) the number of collocation points in the Legendre collocation method (triangles), (2) the number of intervals in the semi-discretization method (squares), and (3) the order of the Lagrange trial functions of the spectral element method (dots).

5. Conclusions

In this paper, the implementations of the semi-discretization, spectral element, and Legendre collocation methods were presented and contrasted. While each of these methods has been used to study various DDEs, a comparison amongst these methods has yet to appear in the literature. The methods were compared for relative convergence rate and computational time using three numerical studies consisting of a ship stability example, the delayed damped Mathieu equation, and a helicopter rotor control problem.

The semi-discretization method is based on discretizing the period and delay into uniform intervals. Because this method relies on increasing the number of uniform intervals to reach convergence, it is expected that the method will converge at a linear rate (i.e. "*h*-convergence") even for higher order implementations. Both the spectral element and Legendre collocation methods rely on increasing the order of the polynomials to achieve convergence. It is therefore

Table 3
The minimum computational dimension to achieve convergence and the computational time required to calculate the stability diagram for Eq. (38). The computational time for each method was calculated for the associated computation dimension in the table.

Method	Computational dimension	Computational time (s)
$\mu = 0.3$		
Semi-discretization	35+	115.2
Spectral element	20	41.9
Legendre collocation	35	38.0
$\mu = 0.75$		
Semi-discretization	42+	184.1
Spectral element	27	88.7
Legendre collocation	42	57.0
$\mu = 1.2$		
Semi-discretization	45+	200.9
Spectral element	29	101.3
Legendre collocation	45	66.6

expected that these methods will converge exponentially (i.e. "*p*-convergence"). Both expectations were realized in the numerical studies. The semi-discretization method demonstrated a linear rate of convergence, while both the spectral element and Legendre collocation methods converged at an exponential rate.

We used three numerical studies with second order, continuous, linear, single-delayed differential equations to compare the convergence rate and the relative computational time between the Legendre collocation, semi-discretization, and spectral element methods. We found the spectral element method to have the quickest convergence rate for all three studies, but the Legendre collocation method had the shortest computational time. The semi-discretization method did not converge when using less than 50 intervals for any of the numerical studies and required the longest computational for all three studies.

In cases where the convergence rate is the most important aspect, the spectral element method should clearly be used. In the studies, the spectral element method converged with about a 36 percent smaller computational dimension than the Legendre collocation method. In computational terms, a quicker convergence rate leads to using less memory for calculations. Smaller computational dimensions results in smaller monodromy matrices which leads to using less memory. Memory usage is an important factor for high dimensional systems or complicated systems that require a finer mesh.

In cases where memory is not an issue, the Legendre collocation method becomes attractive because of its relative speed. The Legendre collocation method requires fewer calculations than the spectral element method and therefore tends to require less computational time. For all three studies, the Legendre collocation method was about 10–56 percent faster than the spectral element method.

In this paper all examples assumed that the delay was equal to the period (i.e. $\tau = T$). Systems do exist where the delay is several periods long, distributed, or arbitrary. For instance, the DDME in Section 4.2 can be implemented using long or arbitrary delays. However, including long, distributed, or arbitrary delays complicates the comparison between the methods and are out of the scope of this paper. The semi-discretization method [41] and spectral element method [42] are capable of handling long, distributed, and arbitrary delays. The authors are not aware of a paper extending the Legendre collocation method to arbitrary delays, but it could be extended by implementing the same techniques used for the spectral method. Future studies in which long, distributed, and arbitrary delays are compared would be a welcome follow-up to this paper.

Acknowledgment

The authors would like to acknowledge financial support from the US National Science Foundation through Grant no. CMMI-0900266.

References

[1] G. Stépán, Delay-differential equation models for machine tool chatter, in: *Dynamics and Chaos in Manufacturing Processes*, 1st ed., Wiley, New York, 1997, pp. 165–192.
[2] J.K. Hale, S.V. Lunel, *Introduction to Functional Differential Equations*, Springer-Verlag, New York, 1993.
[3] J. Bailey, W. Haddad, Drug dosing control in clinical pharmacology, *IEEE Control Systems Magazine* 25 (2005) 35–51.
[4] D. Seo, C. Chicone, Z. Feng, Synchronization problem in delay-line oscillator saw sensors, *Sensors and Actuators A: Physical* 121 (2005) 44–51 http://dx.doi.org/10.1016/j.sna.2005.02.002.
[5] C. Chicone, Z. Feng, Synchronization phenomena for coupled delay-line oscillators, *Physica D: Nonlinear Phenomena* 198 (3–4) (2004) 212–230. http://dx.doi.org/10.1016/j.physd.2004.08.027.
[6] A. Verdugo, R. Rand, Hopf bifurcation in a DDE model of gene expression, *Communications in Nonlinear Science and Numerical Simulation* 13 (2008) 242–325. http://dx.doi.org/10.1016/j.cnsns.2006.05.001.

[7] N. Olgac, B. Holm-Hansen, A novel active vibration absorption technique: delayed resonator, *Journal of Sound and Vibration* 176 (1) (1994) 93–104. http://dx.doi.org/10.1006/jsvi.1994.1360.
[8] N. Olgac, E. Elmali, S. Vijayan, Introduction to the dual frequency fixed delayed resonator, *Journal of Sound and Vibration* 189 (3) (1996) 355–367. http://dx.doi.org/10.1006/jsvi.1996.0024.
[9] M. Hosek, H. Elmali, N. Olgac, A tunable torsional vibration absorber: the centrifugal delayed resonator, *Journal of Sound and Vibration* 205 (2) (1997) 151–165. http://dx.doi.org/10.1006/jsvi.1997.0996.
[10] O. Bobrenkov, F. Khasawneh, E. Butcher, B. Mann, Analysis of milling dynamics for simultaneously engaged cutting teeth, *Journal of Sound and Vibration* 329 (5) (2010) 585–606. http://dx.doi.org/10.1016/j.jsv.2009.09.032.
[11] N. Sims, B. Mann, S. Huyanan, Analytical prediction of chatter stability for variable pitch and variable helix milling tools, *Journal of Sound and Vibration* 317 (2008) 664–686. http://dx.doi.org/10.1016/j.jsv.2008.03.045.
[12] T. Insperger, B.P. Mann, G. Stépán, P.V. Bayly, Stability of up-milling and down-milling, Part 1: alternative analytical methods, *International Journal of Machine Tools and Manufacture* 43 (2003) 25–34.
[13] Y. Altintas, E. Budak, Analytical prediction of stability lobes in milling, *CIRP Annals* 44 (1995) 357–362.
[14] H. Ma, E. Butcher, Stability of elastic columns with periodic retarded follower forces, *Journal of Sound and Vibration* 286 (2005) 849–867. http://dx.doi.org/10.1016/j.jsv.2004.10.052.
[15] G. Stépán, *Retarded Dynamical Systems: Stability and Characteristic Functions*, John Wiley & Sons, 1989.
[16] D. Breda, S. Maset, R. Vermiglio, Pseudospectral differencing methods for characteristic roots of delay differential equations, *SIAM Journal of Scientific Computing* 27 (2) (2005) 482–495. http://dx.doi.org/10.1137/030601600.
[17] J.-Q. Sun, B. Song, Optimal control of time-delayed linear systems with the method of continuous time approximation, *ASME Conference Proceedings* 2008 (43321) (2008) 317–322. http://dx.doi.org/10.1115/SMASIS2008-388.
[18] J.-Q. Sun, A method of continuous time approximation of delayed dynamical systems, *Communications in Nonlinear Science and Numerical Simulation* 14 (4) (2009) 998–1007. http://dx.doi.org/10.1016/j.cnsns.2008.02.008.
[19] N. Olgac, R. Sipahi, A unique methodology for chatter stability mapping in simultaneous machining, *Journal of Manufacturing Science and Engineering* 127 (2005) 791–800. http://dx.doi.org/10.1115/1.2037086.
[20] R. Sipahi, N. Olgac, Complete stability analysis of neutral-type first order two-time delay systems with cross-talking delays, *SIAM Journal on Control and Optimization* 45 (3) (2006) 957–971. http://dx.doi.org/10.1137/050633810.
[21] T. Insperger, G. Stépán, Semi-discretization method for delayed systems, *International Journal for Numerical Methods in Engineering* 55 (2002) 503–518. http://dx.doi.org/10.1002/nme.505.
[22] T. Insperger, G. Stépán, Updated semi-discretization method for periodic delay-differential equations with discrete delay, *International Journal for Numerical Methods in Engineering* 61 (2004) 117–141. http://dx.doi.org/10.1002/nme.1061.
[23] T. Insperger, G. Stépán, J. Turi, On the higher-order semi-discretizations for periodic delayed systems, *Journal of Sound and Vibration* 313 (2008) 334–341. http://dx.doi.org/10.1016/j.jsv.2007.11.040.
[24] J.P. Boyd, *Chebyshev and Fourier Spectral Methods*, Dover Publications, 2001.
[25] B. Mann, B. Patel, Stability of delay equations written as state space models, *Journal of Vibration and Control* 16 (2010) 1067–1085. http://dx.doi.org/10.1177/1077546309341111.
[26] F.A. Khasawneh, B.P. Mann, A spectral element approach for the stability of delay systems, *International Journal for Numerical Methods in Engineering* (2011) 566–592. http://dx.doi.org/10.1002/nme.3122.
[27] F. Khasawneh, D. Barton, B. Mann, Periodic solutions of nonlinear delay differential equations using spectral element method, *Nonlinear Dynamics* 67 (1) (2011) 641–658. http://dx.doi.org/10.1007/s11071-011-0017-3.
[28] F. Khasawneh, B. Mann, Stability of delay integro-differential equations using a spectral element method, *Mathematical and Computer Modelling* 54 (2011) 2493–2503. http://dx.doi.org/10.1016/j.mcm.2011.06.009.
[29] F. Khasawneh, B. Mann, E. Butcher, A multi-interval Chebyshev collocation approach for the stability of periodic delayed systems with discontinuities, *Communications in Nonlinear Science and Numerical Simulation* 16 (2011) 4408–4421. http://dx.doi.org/10.1016/j.cnsns.2011.03.025.
[30] W. Brogan, *Modern Control Theory*, Prentice Hall, 1991.
[31] J. Berrut, L.N. Trefethen, Barycentric Lagrange interpolation, *SIAM Review* 46 (3) (2004) 501–517. http://dx.doi.org/10.1137/S0036144502417715.
[32] N. Higham, The numerical stability of barycentric Lagrange interpolation, *IMA Journal of Numerical Analysis* 24 (4) (2004) 547–556. http://dx.doi.org/10.1093/imanum/24.4.547, arXiv: 〈http://imajna.oxfordjournals.org/cgi/reprint/24/4/547.pdf〉.
[33] J. Reddy, *An Introduction to the Finite Element Method*, 2nd ed., McGraw-Hill, Inc., New York, NY, 1993.
[34] S. Parter, On the Legendre–Gauss–Lobatto points and weights, *Journal of Scientific Computing* 14 (4) (December 1999). 347–355(9), http://dx.doi.org/10.1023/A:1023204631825.
[35] N. Minorsky, Self excited oscillations in systems possessing retarded actions, *Journal of Applied Mechanics* 9 (1942) 65–71.
[36] N. Minorsky, *Nonlinear Oscillations*, D. Van Nostrand Company, Inc., 1962.
[37] T. Insperger, G. Stepan, Stability chart for the delayed Mathieu equation, *Proceedings of Royal Society of London A* 458 (2002) 1989–1998. http://dx.doi.org/10.1098/rspa.2001.0941.
[38] T. Insperger, G. Stepan, Stability of the damped Mathieu equation with time delay, *Journal of Dynamic Systems, Measurement, and Control* 125 (2003) 166–171. http://dx.doi.org/10.1115/1.1567314.
[39] P. Arcara, S. Bittanti, M. Lovera, Periodic control of helicopter rotors for attenuation of vibrations in forward flight, *IEEE Transactions on Control Systems Technology* 8 (6) (2000) 883–894. http://dx.doi.org/10.1109/87.880590.
[40] R. Pandiyan, S. Sinha, Periodic flap control of a helicopter blade in forward flight, *Journal of Vibration and Control* 5 (1999) 761–777. http://dx.doi.org/10.1177/107754639900500506.
[41] T. Insperger, G. Stépán, *Semi-Discretization for Time-delay Systems: Stability and Engineering Applications (Applied Mathematical Sciences)*, Springer, New York, 2011.
[42] F. Khasawneh, B. Mann, A spectral element approach for the stability analysis of time-periodic delay equations with multiple delays, *Journal of vibration and acoustics* (2010).